Theoretical investigation of refractive index detection limit in the Surface Plasmon Resonance-triggered switch effect

Hugo Bruhier, Isabelle Verrier, Jérôme Brunet, Christelle Varenne, Frédéric Celle, Yves Jourlin

Theoretical investigation of refractive index detection limit in the Surface Plasmon Resonance-triggered switch effect

Hugo Bruhier, Isabelle Verrier, Jérôme Brunet, Christelle Varenne, Frédéric Celle and Yves Jourlin

***Abstract*—The metrological performances of a SPR-based sensor exploiting the plasmon-triggered switch effect are investigated in this article. The switch effect, recently demonstrated, is a lossless energy transfer phenomenon between the 0th and -1st diffracted orders, through SPR excited modes, which only occurs in a deep metallic grating while the incidence angle or the wavelength varies. A differential measurement of diffraction efficiencies of these two propagative diffracted orders and an optimized signal filtering, allows to retrieve the sensing signal at a fixed wavelength or fixed incidence angle. For a deep metallic grating illuminated under TM polarization, such a sensor provides a high sensitivity and a limit of detection lower than 10^{-7} RIU reaching thus the limits of the best current plasmonic methods. The theoretical sensitivity and measurement uncertainties are rigorously investigated considering digital signal processing in order to provide an optimized signal processing and thus increase the sensitivity and the current Limit of Detection (LOD). Due to its performances and its implementation simplicity, this new SPR based sensor is very promising for the detection and quantification of chemical and biological species both in liquid and gaseous environments.**

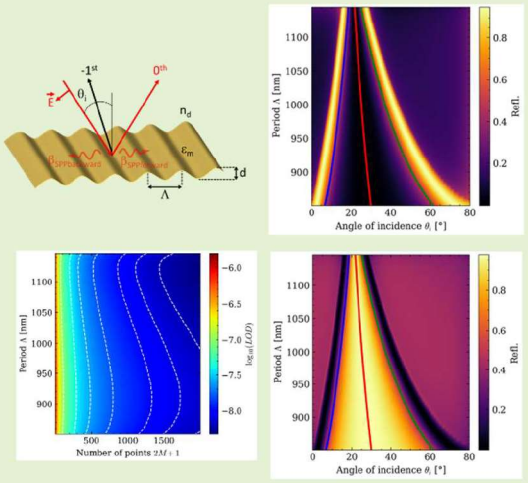

***Index Terms*— Gratings, optical sensor, plasmons, refractive index measurement.**

I. Introduction

TODAY, numerous methods using surface plasmons resonance (SPR) are widely investigated for the detection of various molecules such as gaseous [1], [2], chemical [3] or biological compounds [4]. SPR can also be used in several fields [5] such as electrochemistry [6] or in systems intended to measure physical quantities like temperature [7], refractive index [8] or detect condensation phenomena [9]. Some techniques use localized plasmons [10] including nanoparticles [11], [12] or waveguides [13], [14], [15], [16] and are able to provide information on the nature and concentration of identified species with high selectivity and sensitivity. The plasmon-based biosensors can also be advantageously arranged in such a way as to detect several species simultaneously [17], [18]. Several works have focused on determining, comparing [19], analyzing [20], [21], [22], [23], [24] and improving [25], [26], [27] the sensitivities of different surface plasmons-based bio-detection devices indeed. Limit of detection (LOD) approaching 10^{-8} Refractive Index Unit have been achieved [25], [28], [29], suggesting the possibility to detect tiny quantities of targeted species.

The work reported here is also based on the SPR approach but involves an effect, called plasmon-triggered optical switching, obtained through the exploitation of the two diffraction orders -1st and 0th of a deep metallic grating. The plasmon-triggered optical switching was recently demonstrated experimentally and theoretically by the research team of the present paper [30], [31], [32] and used as a probe effect to perform refractive index measurements in aqueous [33] (for biosensing application [34]) and gaseous [35] environments and have shown potentialities in the measurement of magnetic field [36]. To go further and for optimization, study of the theoretical limitations of this effect is necessary and will highlight some parameters to improve the measurements and so to emphasize the use of this effect in sensors systems. The aim of this paper is thus to establish the required conditions to exploit correctly this effect by a judicious and smart choice of the measurement parameters and an adequate processing of the signal. The expected results

This research was funded by the national French research agency in the frame of the CAPTAIN project (grant number ANR-18-CE04-0008).

H. Bruhier is affiliated with both Université Jean Monnet Saint-Etienne, CNRS, Institut d'Optique Graduate School, Laboratoire Hubert Curien UMR CNRS 5516, F-42023, Saint-Etienne and INSA Lyon, CNRS, Université Claude Bernard Lyon 1, MATEIS, UMR 5510, F-69621 Villeurbanne, France; hugo.bruhier@univ-st-etienne.fr.

I. Verrier, F. Celle and Y. Jourlin are affiliated with Université Jean Monnet Saint-Etienne, CNRS, Institut d'Optique Graduate School, Laboratoire Hubert Curien UMR CNRS 5516, F-42023, Saint-Etienne, France; isabelle.verrier@univ-st-etienne.fr; celle@univ-st-etienne.fr; yves.jourlin@univ-st-etienne.fr

C. Varenne and J. Brunet are affiliated with Université Clermont Auvergne, CNRS, Sigma Clermont, Institut Pascal, F-63000 Clermont-Ferrand, France ; jerome.brunet@uca.fr; christelle.varenne@uca.fr

are also pointed out: the sensor sensitivity and LOD are calculated for a simple sensor configuration consisting of a metallic diffraction grating without buffer or functionalized layer in order to compare performance to the state of the art and the previous results.

The first part of this paper is devoted to the comparison of SPR method for shallow and deep metallic gratings used as transducers for refractive index measurements in order to introduce the switch effect exploited in this approach. Angular or spectral interrogation of a media with 0th order resonance tracking is a classical and well-known measurement for years, applied in the case of a shallow grating. For a deep grating, the refractive index change of the media is measured from two diffraction orders intensities by the plasmon-triggered optical switching effect, at the so-called "processing points". The sensing signal output is then the normalized difference of the two diffraction orders intensities and the metrological development over the sensing signal consists in the sensitivity and the uncertainty determination versus the measured quantities leading to the limit of detection (LOD). A low-pass numerical moving average filter is a powerful simple method to reduce the noise.

The second section applies the method previously described to optimized grating parameters that maximize the sensitivity for each grating period. Theoretical sensitivity and uncertainty extracted from experimental noise are computed using different filter window sizes.

Finally, the limit of detection is computed from modeled sensitivities and calculated uncertainties with optimized signal processing parameters leading to theoretical limit of detection at the level of the state of the art.

II. Plasmonic Sensing

A. Surface plasmon resonance and plasmon-triggered optical switching effect

The surface plasmon resonance (SPR) is based on the excitation of a surface wave at a metal/dielectric interface [37], [38] under TM light polarization. Considering the complex permittivity of the metal $\varepsilon_m = \varepsilon'_m + j\varepsilon''_m$, the refractive index of the dielectric medium n_d at the metal-dielectric interface and the light wavenumber $k_0 = \frac{2\pi}{\lambda}$ (λ is the wavelength in nm), the real part of the propagation constant of this surface wave (noted β_{SPP}) can be approximated by [39]:

$$\beta_{SPP} \cong k_0 \sqrt{\frac{\varepsilon'_m n_d^2}{\varepsilon'_m + n_d^2}} \quad (1)$$

which is true for two semi-infinite media with a perfectly flat interface. It is easy to show with this equation that the plasmon mode dispersion lies outside the light cone containing the propagating diffracted orders and must be excited with evanescent waves [40]. One way to excite such plasmonic waves, the first historically one [41], consists of using metallic diffraction gratings. The evanescent diffracted orders under TM polarization can then excite the plasmon surface mode with a phase matching between the plasmon mode momentum and the non-propagative diffracted order. This correspondence between the m^{th} diffracted order and the surface plasmon mode is verified with the grating equation:

$$k_0 n_d \sin(\theta_i) + mK_G = \pm\beta_{SPP} \quad (2)$$

where θ_i stands for the incidence angle on the grating and K_G is the grating vector, defined from the grating period Λ with $K_G = \frac{2\pi}{\Lambda}$ (Figure 1).

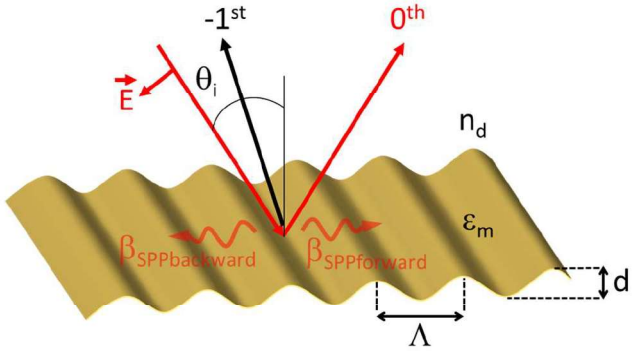

Fig. 1. Excitation of the plasmon surface modes under TM polarization by the evanescent diffracted orders of a grating.

The 0th order reflectivity of a shallow gold sinusoidal diffraction grating (period $\Lambda = 1000$ nm, depth $d = 36$ nm) in vacuum ($n_d = 1$) at a wavelength λ of 850 nm under TM polarization is shown in Figure 2(a). The plasmon resonance excited by the evanescent +1st diffraction order, under an incidence angle of approximately 9.6°, is characterized by a minimum in the reflection, as a dip in the reflection angular spectrum for the resonance angle. The distributed energy of the propagative diffraction orders of the grating at this resonance angular position, *i.e.* the sum of the reflected intensities diffracted by each order represented by a grey dotted line in Figure 2(a) (the electromagnetic balance), tends to 0. The incident energy is thus transferred in the propagative surface plasmonic mode. This reflectivity calculation, as well as the electromagnetic modeling of this work is carried out with the Chandezon method [42], [43] implemented in a commercial software [44].

By increasing the depth of the metallic grating, it is possible to achieve a new effect, the plasmon-triggered optical switching [30]. This effect can be observed under certain conditions: a fairly large grating depth and compliance with the following inequality $3K_G \gtrsim 2\beta_{SPP}$ [31]. The typical grating angular response due to this effect is shown in Figure 2(b) for a deep gold sinusoidal diffraction grating ($\Lambda = 1000$ nm, $d = 290$ nm) at a wavelength of $\lambda = 850$ nm under TM polarization. The angular positions of the reflected 0th order maxima (at around incidence angles of 11° and 42°) correspond to the excitation of a forward (resp. backward) plasmon mode by the evanescent diffracted order +1st (resp. -2nd). One can observe the so-called switch effect for deep gratings with the angular spectrum of Figure 2(b) illustrated by the energy transfer between the 0th and the -1st diffracted orders on each side of the -1st order Littrow angle ($\theta_L = 25°$). The main and astonishing effect of such phenomon is that it is lossless since few energy is absorbed even though plasmonic modes are excited, as it can be seen by the electromagnetic balance, represented with a grey dotted line in Figure 2(b).

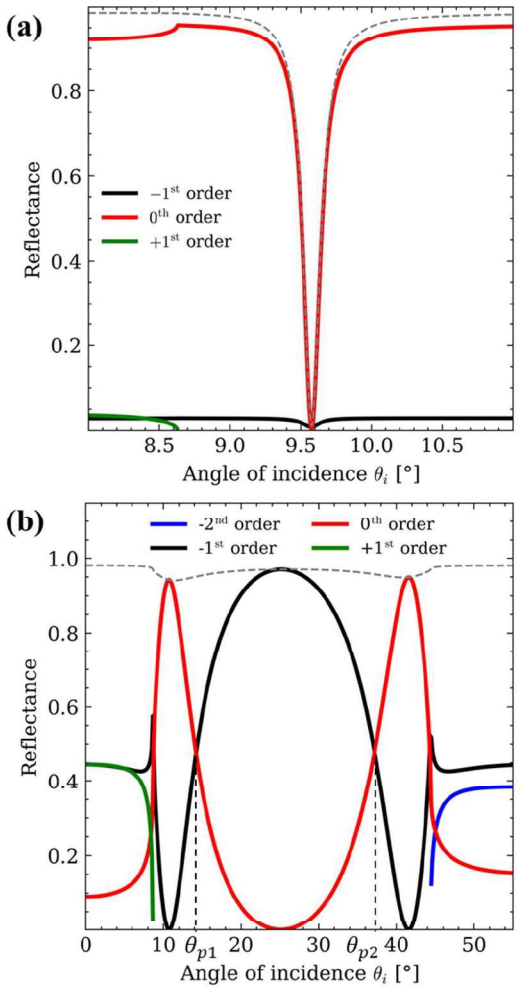

Fig. 2. (a) Reflected -1st and 0th order efficiency of a shallow sinusoidal gold diffraction grating ($\Lambda = 1000$ nm, $d = 36$ nm) in vacuum, illuminated under TM polarization at a wavelength λ of 850 nm. (b) Reflected -2nd, -1st, 0th and +1st orders efficiencies of a deep sinusoidal gold diffraction grating ($\Lambda = 1000$ nm, $d = 290$ nm) in vacuum, illuminated at a wavelength λ of 850 nm in TM polarization. The electromagnetic balance is shown by the grey dotted line.

B. Sensing methods

Refractive index sensing with SPR was extensively studied in the literature [45], [46], [47]. The most common method is to measure the angular position of the 0th order resonance, obtained in the case of a shallow grating, directly linked to the refractive index of the probed medium through (1) and (2). The advantage of this method is that the resonance position depends linearly on the refractive index [48]. However, accurate measurement of the resonance position requires measuring the reflectivity over a certain angular or spectral range and using specific algorithms to recover the position of the minimum. Some algorithms [49], [50] use a wide range of reflectance around the resonance position in order to have a better monitoring over time.

The use of the plasmon-triggered optical switch makes it possible, from a simple measurement and acquisition configuration, with very high sensitivities [33], [35] and to avoid common-mode noise thanks to the differential measurement performed by the normalized difference of the two reflected orders intensities. From the angular response in Figure 2(b), two specific angular positions can be examined: the crossing points of the two diffraction efficiency curves at incidence angles $\theta_{p_1} \cong 14°$ and $\theta_{p_2} \cong 37°$. These points will be named the "processing points" in the following sections. Due to the initial equality of the two diffraction efficiencies, the differential measurement of the two diffracted intensities can be carried out from one of these two processing points and measured over time as a function of the refractive index change of the surrounding medium. When the refractive index of the probed medium changes, the resonance positions (at incidence angles of 11° and 42°) are modified. On the contrary, the central position (at approximately $\theta_L = 25°$), corresponding to the Littrow angle of the -1st order, remains almost unchanged. The angular measurement position remaining fixed at one of the processing points, the modification of the refractive index consequently induces a variation of the two diffracted orders reflectance in an opposite direction. Measuring the differential intensity of these two orders makes possible to follow the refractive index changes. The main advantages of this method are the simplicity of the measurement (monochromatic light source and two photodiodes for the diffraction orders intensities measurement) and the possibility to suppress the time variations of the source light intensity using the differential measurement. The simple difference $\delta(t)$ of the diffracted intensities in the 0th order ($I_0(t)$) and -1st order ($I_{-1}(t)$) is unable to suppress totally the variations of intensity of the light source (equation (3)).

$$\delta(t) = I_0(t) - I_{-1}(t) \tag{3}$$

A better dimensionless quantity, called the "normalized difference" $\mathcal{D}(t)$, inherently suppress the common mode noise and is defined as:

$$\mathcal{D}(t) = \frac{I_0(t) - I_{-1}(t)}{I_0(t) + I_{-1}(t)} \tag{4}$$

This quantity was determined experimentally and showed great sensing performances [35]. In this paper the normalized difference $\mathcal{D}(t)$ will be defined from the measured diffracted intensities for sensitivity analysis or from the diffracted efficiencies for uncertainty analysis, the two formulations being equivalent.

III. Metrological Analysis and Filtering

A. Metrology of the normalized difference and limit of detection

The determination of the limit of detection relative to a sensor requires the knowledge of both the sensitivity of the signal to be measured and its uncertainty. These quantities are obtained as explained into the following paragraphs.

According to our measurement protocol, the sensitivity, unlike other works [25], [26], [51], will not be defined from a variation of the propagation constant of the plasmon mode. Indeed, the approximation of equation (1) for the propagation constant becomes less accurate when the depth of the grating increases [52] and cannot be used in the case of deep gratings, required for the plasmon-triggered optical switch. The sensitivity $\mathcal{S}$ will then be defined in equation (5) simply as:

$$\mathcal{S} = \frac{\partial \mathcal{D}}{\partial n_d} \tag{5}$$

taking the normative definition, i.e. the variation of the measured quantity (the normalized difference ($\delta\mathcal{D}$)) divided by the variation of the measurand (the refractive index of the incident medium (δn_d)).

The uncertainty of an indirect measurement can be evaluated from the uncertainties (the standard deviation) of each measured variables and from their covariances [49], [50]. This method assumes that the obtained signal is linear in the vicinity of the studied point (processing point). The uncertainty $\sigma_{\mathcal{D}}$ of the normalized difference can be then expressed (from equation (4)) from the uncertainties and the covariance of the measured diffraction intensities and is given by:

$$\sigma_{\mathcal{D}} = \frac{2\sqrt{I_{-1}^2\sigma_{I_0}^2 + I_0^2\sigma_{I_{-1}}^2 - 2I_0 I_{-1}\sigma_{I_0 I_{-1}}}}{(I_0 + I_{-1})^2}. \tag{6}$$

This equation shows that the covariance between the two measured signals ($\sigma_{I_0 I_{-1}}$) allows to reduce the uncertainty of the normalized difference. The final quantity to define in order to study the sensing properties of the plasmon-triggered optical switch is the limit of detection (LOD). Several possibilities exist. Considering that the resulting noise on the normalized difference has a Gaussian distribution, taking three times the uncertainty encompasses 99% of the noise, the LOD will be taken in this paper as (eq. (7)):

$$LOD = \frac{3\sigma_{\mathcal{D}}}{\mathcal{S}}. \tag{7}$$

B. Signal filtering

According to equation (7), a way to improve the LOD is the reduction of the normalized difference uncertainty (given in equation (6)) as well as increasing the sensitivity. Concerning the normalized difference uncertainty, the simplest method remains the filtering of the measured signals intensities in order to decrease their noise. The filter used in this work is a numerical low-pass filter: the moving average. The filtering window is centred (non-causal filter) with a window width of $2M+1$ points. In order to study the frequency response, we have to compute the $\mathcal{Z}$ transform [53] of the filter transfer function $\mathcal{H}$ expressed as:

$$\mathcal{H}(\nu) = \frac{1}{2M+1}\left(1 + 2\sum_{l=1}^{M}\cos(2l\pi\nu)\right) \tag{8}$$

with ν the normalized frequency defined for the sampling frequency f_s as $\nu = \frac{f}{f_s}$. The cut-off normalized frequency ν_c, can be computed versus the number of points of the filtering window as shown in Figure 3. The sampling frequency and the filtering window size is a couple of parameters that has to be chosen carefully. For example, a sampling frequency of 500 Hz, a 51 points moving average will result in a cut-off frequency of approximately 3.5 Hz. This cut-off frequency can be considered too low compared to the signal frequency of interest. The moving average filter is implemented with the *uniform_filter1d* function of the *ndimage* module of the SciPy python library [54] using *reflect* mode for boundary conditions. In this study, to avoid possible long-time variations of the measured signals a high-pass filtering is also implemented. The filter is the simplest one presented in [55] and its parameters wisely chosen in order to suppress the 50 Hz line frequency electrical noise .

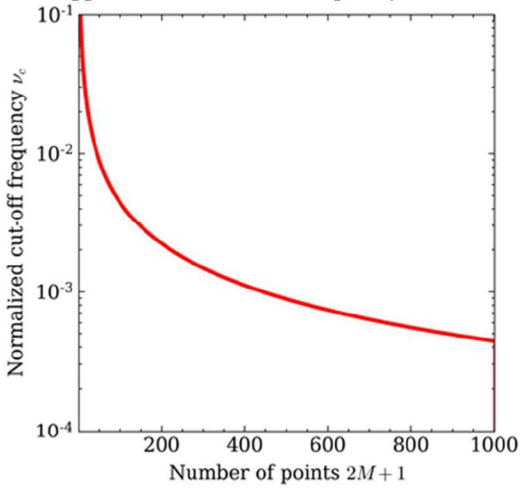

Fig. 3. Normalized cut-off frequency (at -3 dB) of the moving average filter (equation (8)) versus the total number of points used to compute the moving average.

IV. Results and Discussion

A. Computed sensitivity

The numerical analysis focuses on the study of a gold grating with a perfect sinusoidal profile put in vacuum at a wavelength $\lambda = 850$ nm under TM polarization. At this wavelength the permittivity of gold is equal to $\varepsilon_m = -32.015 + 1.2565\,j$ [56]. The analysis is performed over a wide range of periods for that wavelength. In order to compare each structure, it appears necessary to find an optimized depth of the grating structure for each period. This optimized depth allows to set the maxima of the 0th order at the two resonances angle positions (at incidence angles of 11° and 12° in Figure 2(b)) and a minimum for this same reflected order at the -1st order Littrow angle (at 25° in Figure 2(b)), which position depends on the period of the grating. The optimized depth calculated for each period is reported in Figure 4(a). The period range is limited by the fact that the angular response becomes too wide (resp. narrow) for low (resp. high) period values. Over all the considered period range, the ratio between the period of the grating and the optimized depth remains between 3.05 and 3.65, which are amply achievable values for fabrication processes such as Laser Interference Lithography for the grating printing. Using the values of each period/depth couple it is possible to calculate the angular response and therefore the angular positions of the Littrow angle as well as the two processing points corresponding to the angular positions θ_{p_1} and θ_{p_2} illustrated in Figure 2(b). These calculated positions are reported in Figure 4(b).

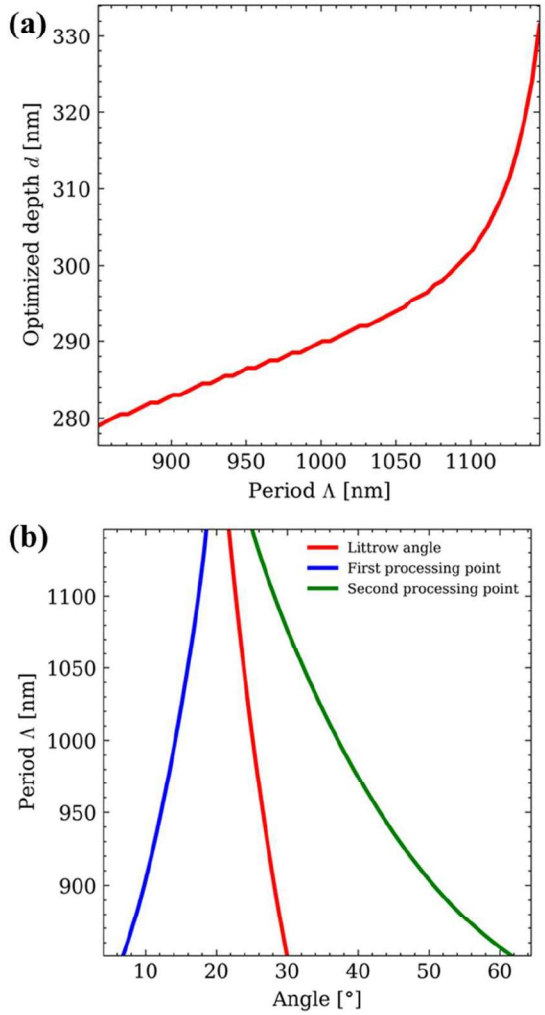

Fig. 4 (a) Optimized modelled depth versus period for the optical switching with a gold grating in vacuum under TM polarization at a wavelength λ of 850 nm. (b) -1st Littrow angle and processing points positions for the different periods associated to depths presented in Figure 3(a).

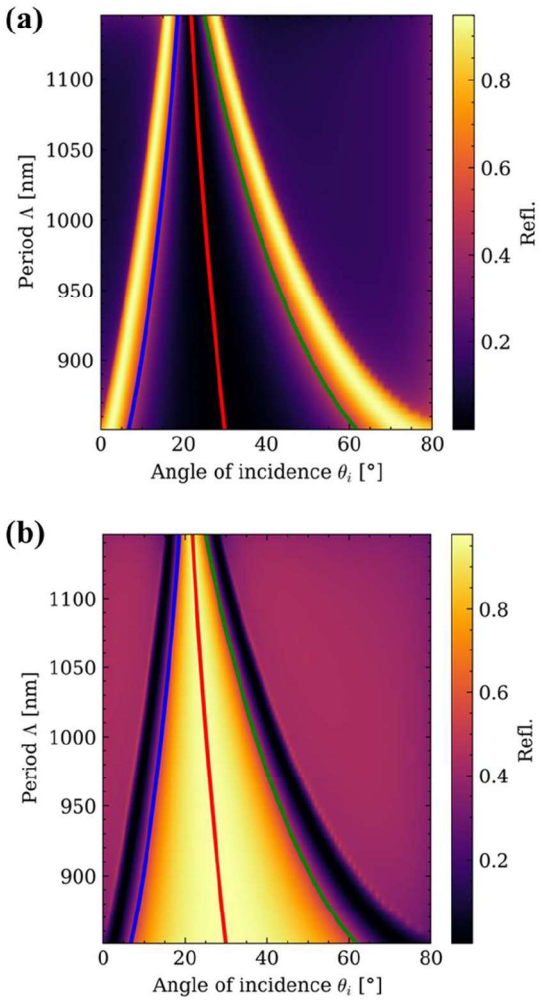

Fig. 5. Angular modelled reflectance in vacuum of the (a) 0th and (b) -1st diffracted orders for a gold sinusoidal grating versus the period associated to the depths found in Figure 4(a) under TM polarization at $\lambda = 850$ nm with the angular positions of Figure 4(b).

In order to have a better analysis of the angular responses of the structures, the 0th and -1st orders diffraction efficiencies are plotted in Figure 5(a) and Figure 5(b) respectively, with the angular positions extracted from the Figure 4(b). For each period, the shape of the angular response of the plasmon-triggered switching effect is met (as the angular response of the Figure 2(b)).

The study of the plasmon-triggered switching effect sensitivity requires to compute the diffraction efficiencies (*i.e.* the diffracted intensities) of the two reflected orders at the two processing points and to characterize the normalized difference (defined in equation (4)) variation as a function of the incident medium refractive index change. This incident medium is considered at the beginning as vacuum ($n_d = 1$) and its refractive index increases by a quantity Δn_d to evaluate the sensitivity. At first, the normalized difference is calculated for each period (Figure 4(b)) from the computed diffraction efficiencies at the two processing points considering vacuum as the incident medium. Then for a change of refractive index Δn_d, the 0th and-1st orders angular spectra (diffraction efficiencies) are modified and the normalized difference is computed for each refractive index value. This calculation is carried out for each period on 5 points between $\Delta n_d = 0$ and $\Delta n_d = 10^{-3}$ RIU. Finally, the sensitivity is computed for each period from equation (5) using each computed normalized difference versus the corresponding refractive index and is plotted in Figure 6 for the first processing point (FPP) and the second processing point

(SPP). The sensitivity value is then comprised between 16 and 25 RIU, despite the different angular extent of the optical responses (see Figure 5(a) and Figure 5(b)).

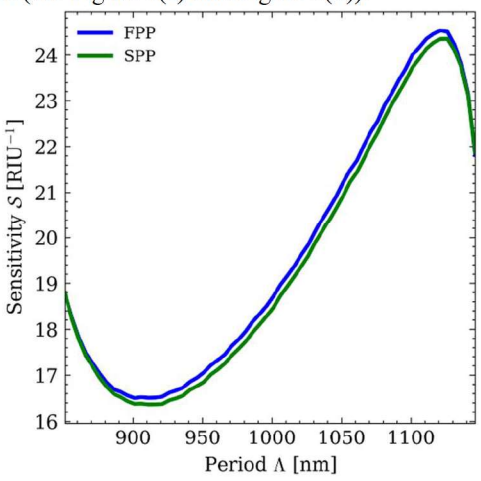

Fig. 6. (a) Sensitivity of the plasmon-triggered optical switch at the two processing points (first processing point – FPP, second processing point SPP) versus the gold grating period, under TM polarization at $\lambda = 850$ nm for the optimized structures with corresponding depths given in Figure 4(a).

A second characteristic of these curves is that the sensitivity is independent of the choice of the processing point and does not depend linearly on the period. It can be counter-intuitive that the sensitivity seems nearly independent from the period of the grating structure [57], [58] and of the plasmonic mode excitation order [59], which is different for the two processing points. This can be explained by the fact that the sensitivity in this configuration is a function of the modification of the angular resonance position and also on the slopes of the diffraction efficiency curves at the processing point positions. At the second processing point, for each period the change of angular position is greater than the one corresponding to the first processing point as it is shown in Figure 7(a), that would be explained by the fact that the first (resp. the second) processing point corresponds to an excitation of the plasmon through the +1st (resp. -2nd) diffraction order. Nevertheless, the slope of the diffraction efficiency curves from the second processing point is lower than that determined at the first processing point (see Figure 7(b)). The same explanation can justify the low modification of the sensitivity by modifying the period of the structure.

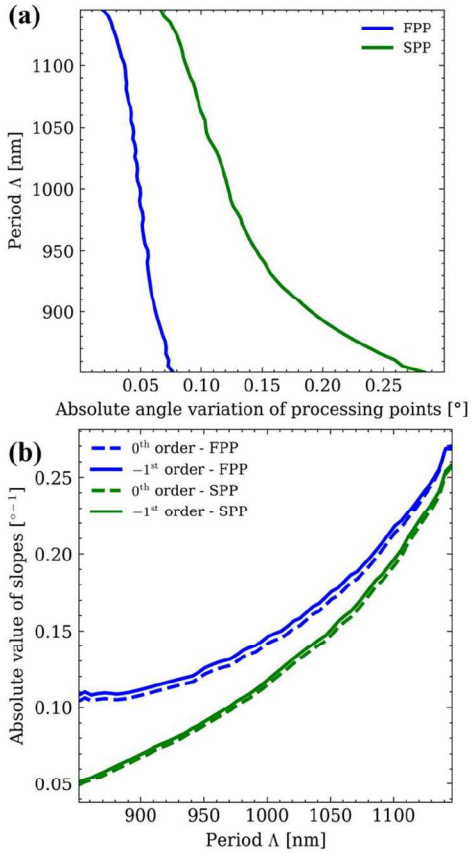

Fig. 7. (a) Modification of the angular position of the two processing points (first processing point – FPP, second processing point SPP) depending of the period of the considered grating structure with an increase of the refractive index of $\Delta n_d = 10^{-3}$. (b) Absolute value of the slopes of the two diffractive orders at the two processing points.

Moreover, the detection range of this plasmon-triggered optical switch measurement set-up is also studied at the wavelength of 850 nm. With this objective, the refractive index variation Δn_d is increased from 10^{-5} RIU to 1 with 4 points by decades, the sensitivity analysis is performed and the regression coefficient R^2 is calculated until it becomes non-linear. The limit value for this non linearity is arbitrarily taken at 0.998 and leads to a detection range up to approximatively 4×10^{-2} RIU regardless of the diffracted structure period. This confirms the initial choice of $\Delta n_d = 10^{-3}$ RIU as the maximum refractive index variation for sensitivity computation.

B. Noise analysis and limit of detection computation

The previous sensitivity analysis provided in the previous section is not sufficient in itself to compute the limit of detection (see equation (7)) and the uncertainty associated with the normalized difference measurement has also to be determined.

In order to assess the electronic intrinsic noise, the measurements are realized without any laser source in a dark room. The measured voltages, corresponding to the diffraction intensities of the two reflected orders (0th and -1st) in equation (4), come from photodiodes (ref. BPW 34 FA) associated with a current-to-voltage converter (ref. NI 9215), a transimpedance circuit, using JFET entry operational amplifier (ref.

AD711JN/TL071) as a current to voltage converter. The analog/digital converter (ADC) allows simultaneous measurements with a 16 bits resolution converter associated to an input range from -10V to +10V. In order to study statistically the signals, the voltage values are measured at 4.6 kHz sampling frequency during 200 s (*i.e.* around 920 ksamples). The value of the sampling frequency was determined according to the number of points for the low-pass filter while keeping a reasonable processing time. After the measurement, the signals are filtered with the low-cut filter of 90 Hz cut-off frequency, presented in subsection 3.2. The signals measured by the two photodiodes are shown in Figure 8(a). A computation of the two photodiodes signal variance gives values equal to 1.71×10^{-6} V² and 1.29×10^{-6} V² respectively, corresponding to a standard deviation of nearly to 1 mV. Covariance between these two signals of 1.40×10^{-6} V² was quantified. This relatively high covariance value (compared to the signals variance) is highlighted by the bivariate plot of Figure 8(b).

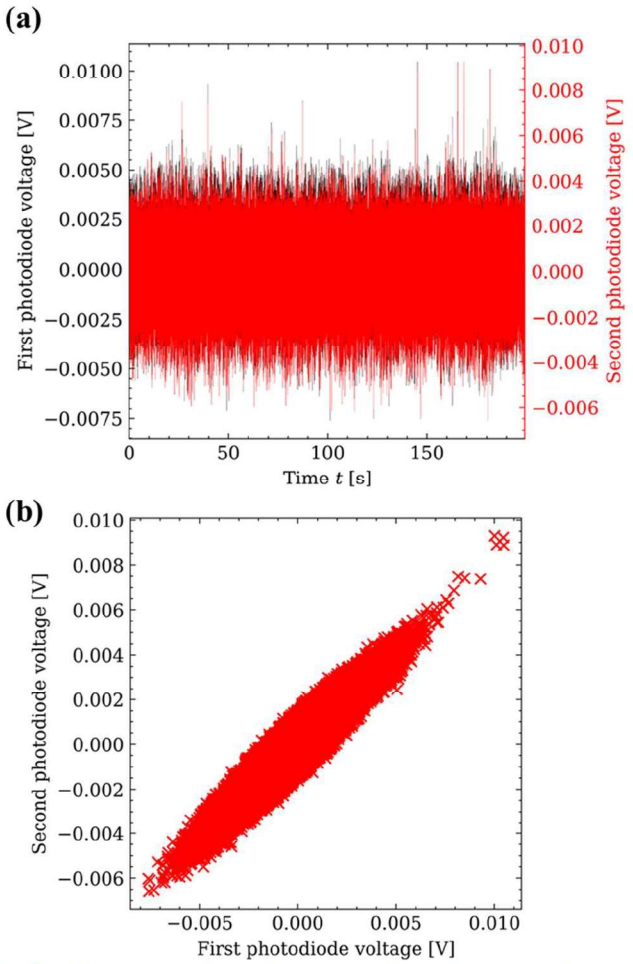

Fig. 8. (a) Measured signals by the two photodiodes at a 4.6 kHz sampling frequency without laser source nor light in the room. (b) Bivariate plot of the two photodiodes signals.

These two signals are then filtered with the moving average filter with the transfer function given in equation (8) with different windows in order to study the effect of the window width. The standard deviation and the covariance of the two filtered signals are plotted in Figure 9(a) and Figure 9(b) for a maximum window filter size of 2000 points.

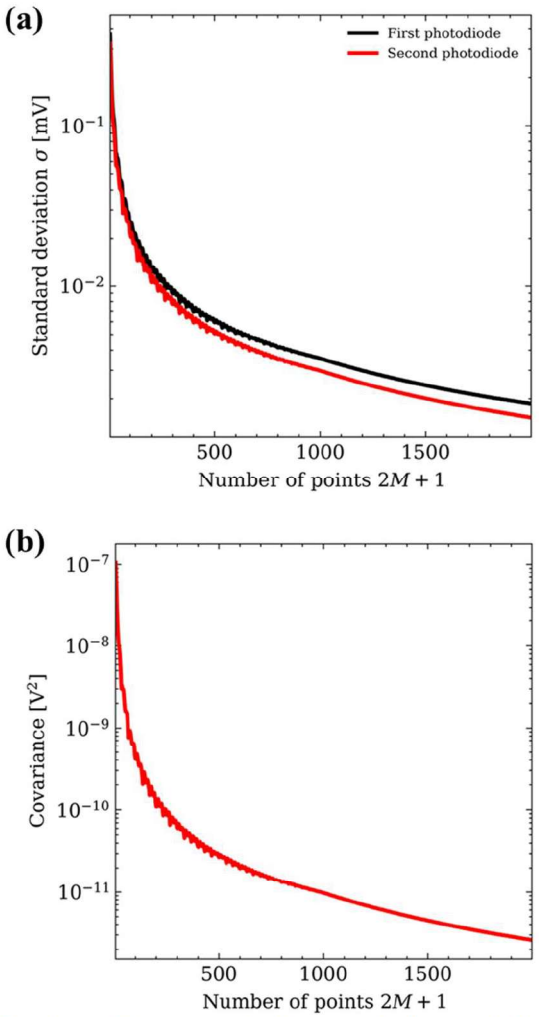

Fig. 9. Variations of the (a) standard deviation for the two photodiode signals and (b) covariance between these signals versus the number of points of the moving average filter.

To compute the uncertainty $\sigma_{\mathcal{D}}$ associated to the normalized difference $\mathcal{D}$ using the equation (6), the diffracted intensities are deduced from voltage signals given by photodiodes. From the equation, it is manifest that the higher the value is, the smaller the normalized difference uncertainty is. The ADC used in this work is limited to a maximum voltage of 10 V as a common specification of most of commercial ADC. The normalized difference uncertainty is thus computed for different window sizes using 10 V for each signal (Figure 10). The curve shape is the same as the ones of the standard deviation and covariance curves of Figure 9(a) and Figure 9(b).

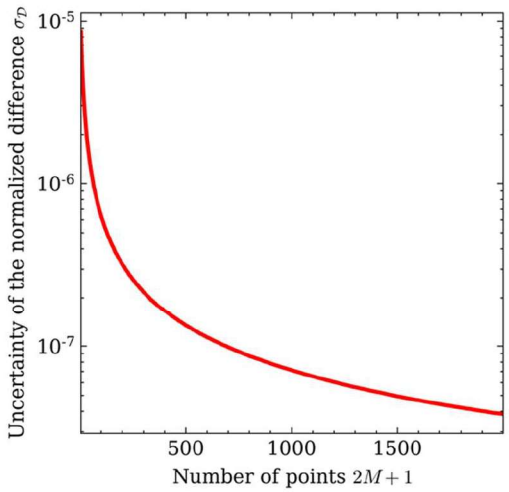

Fig. 10. Uncertainty of the normalized difference (equation (6)) versus the number of points of the moving average filter with values of Figure 9(a) and Figure 9(b) for the uncertainty value of the electrical signals and a voltage value of 10 V.

The detection limit defined by equation (7) can be now computed from each uncertainty value and from each sensitivity value given in Figure 6. The sensitivity, which is a parameter depending on the diffraction efficiency (that is the grating response), is dependent of the grating period and the uncertainty of the sensing signal is linked to the measurement set-up as well as to the signal processing (filtering window width). These two dependencies and values from Figure 6 and Figure 10 will define the limit of detection. Since the sensitivity is the same for the two processing points, the LOD is plotted in Figure 11 for the second processing point, which was the one used in experimental studies [33], [35]. These LOD values show very good results, lower than 10^{-7} RIU for filter window width lower than 100 points, which corresponds to the value of the state of the art for most current plasmonic sensors.

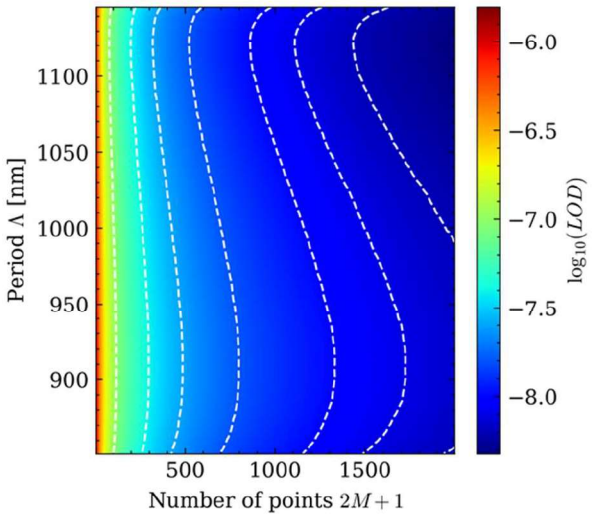

Fig. 11. Limit of detection decimal logarithm computed using equation (7) with modelled sensitivities presented in Figure 6 and normalized difference uncertainties in Figure 10 versus the period and the points number of the low-pass filter at the second processing point for a gold grating at $\lambda = 850$ nm wavelength with optimized depths found in Figure 4(a) and with a 10 V voltage measurement for the diffraction intensities. Contour lines correspond to values [-7, -7.4, -7.6, -7.8, -8, -8.1, -8.2].

The detection limits of classical SPR sensors were already studied theoretically and a work from Piliarik and Homola [26] computed the ultimate resolution of classical SPR sensors (bare metallic layer onto a prism or bare metallic shallow diffraction grating). The cited work gives a theoretical detection limit of value 9×10^{-8} RIU at the wavelength of 850 nm, and the cited studies never overcome this limit whatever the detection method. As the limit was computed in this case for a temporal average over 100 points and considering 400 points for the reflectivity (angular/spectral response), we compared our results to this reference for a filtering window of 99 points and 199 points (temporal average) in Figure 12. We show here that our method, with a simple sensing configuration and low-cost components (photodiodes, transimpedance circuits and ADC), reaches better performance than the detection limit of classical SPR sensors, even when a complex sensing method is used.

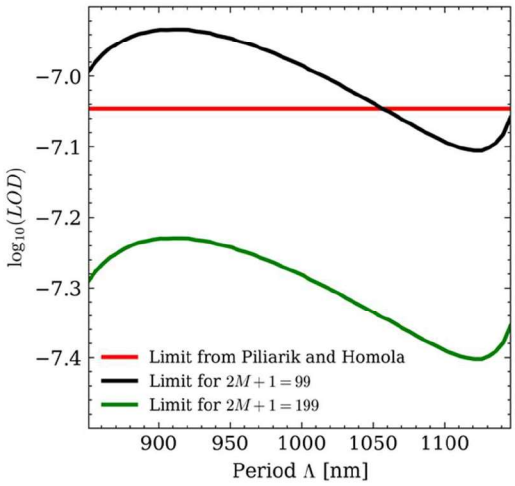

Fig. 12. Computed limit of detection for 99 (in black) and 199 (in green) points for the moving average filter in function of the period compared to the detection limit given in [26] for 100 points of temporal average at wavelength 850 nm.

V. Conclusion

The theoretical performances of a refractive index sensor based on the plasmon-triggered switching effect are investigated here by optimizing both the grating and signal processing parameters. Its principle is based on the differential measurement of the two 0^{th} and -1^{st} orders diffracted by a deep metallic grating. For 850 nm wavelength, its sensitivity varies between 16 and 24 RUI^{-1} depending on the diffraction grating period over an index range of 4 10^{-2}. The corresponding limit of detection (LOD) is less than 10^{-7} RIU after digital filtering (less than 100 points for the filtering window). Thus, the device shows its ability to compete with the best plasmonic sensors while remaining extremely simple to implement: a laser diode and two photodiodes with suitable signal processing. This new generation of SPR based sensors can be used for different applications in liquid or gaseous media and it opens up new possibilities for the detection of biological or chemical species.

Acknowledgment

The authors want to acknowledge Prof. Olivier Parriaux, professor emeritus of Université Jean Monnet, for the fruitful discussions on the plasmon-triggered optical switching effect.

References

[1] R. S. El Shamy, D. Khalil, et M. A. Swillam, « Mid Infrared Optical Gas Sensor Using Plasmonic Mach-Zehnder Interferometer », *Sci Rep*, vol. 10, nº 1, p. 1293, déc. 2020, doi: 10.1038/s41598-020-57538-1.

[2] B. Liedberg, C. Nylander, et I. Lunström, « Surface plasmon resonance for gas detection and biosensing », *Sensors and Actuators*, vol. 4, p. 299-304, janv. 1983, doi: 10.1016/0250-6874(83)85036-7.

[3] Z. Khajemiri, D. Lee, S. M. Hamidi, et D.-S. Kim, « Rectangular plasmonic interferometer for high sensitive glycerol sensor », *Sci Rep*, vol. 9, nº 1, p. 1378, déc. 2019, doi: 10.1038/s41598-018-37499-2.

[4] A. G. Brolo, « Plasmonics for future biosensors », *Nature Photon*, vol. 6, nº 11, p. 709-713, nov. 2012, doi: 10.1038/nphoton.2012.266.

[5] P. Berini, « Surface plasmon photodetectors and their applications », *Laser & Photonics Reviews*, vol. 8, nº 2, p. 197-220, mars 2014, doi: 10.1002/lpor.201300019.

[6] J. G. Gordon et S. Ernst, « Surface plasmons as a probe of the electrochemical interface », *Surface Science*, vol. 101, nº 1-3, p. 499-506, déc. 1980, doi: 10.1016/0039-6028(80)90644-5.

[7] J. Ibrahim *et al.*, « Surface plasmon resonance based temperature sensors in liquid environment », *Sensors (Switzerland)*, vol. 19, nº 15, 2019, doi: 10.3390/s19153354.

[8] H. Wang, « Plasmonic refractive index sensing using strongly coupled metal nanoantennas: nonlocal limitations », *Sci Rep*, vol. 8, nº 1, p. 9589, déc. 2018, doi: 10.1038/s41598-018-28011-x.

[9] J. Ibrahim *et al.*, « Condensation phenomenon detection through surface plasmon resonance », *Optics Express*, vol. 25, nº 20, p. 24189-24198, 2017, doi: 10.1364/OE.25.024189.

[10] H. M. Hiep *et al.*, « A localized surface plasmon resonance based immunosensor for the detection of casein in milk », *Science and Technology of Advanced Materials*, vol. 8, nº 4, p. 331-338, janv. 2007, doi: 10.1016/j.stam.2006.12.010.

[11] I. Reinhard, K. Miller, G. Diepenheim, K. Cantrell, et W. P. Hall, « Nanoparticle Design Rules for Colorimetric Plasmonic Sensors », *ACS Appl. Nano Mater.*, vol. 3, nº 5, p. 4342-4350, mai 2020, doi: 10.1021/acsanm.0c00475.

[12] T. Xie, C. Jing, et Y.-T. Long, « Single plasmonic nanoparticles as ultrasensitive sensors », *Analyst*, vol. 142, nº 3, p. 409-420, 2017, doi: 10.1039/C6AN01852A.

[13] O. Krupin, H. Asiri, C. Wang, R. N. Tait, et P. Berini, « Biosensing using straight long-range surface plasmon waveguides », *Opt. Express*, vol. 21, nº 1, p. 698, janv. 2013, doi: 10.1364/OE.21.000698.

[14] O. Krupin, C. Wang, et P. Berini, « Selective capture of human red blood cells based on blood group using long-range surface plasmon waveguides », *Biosensors and Bioelectronics*, vol. 53, p. 117-122, mars 2014, doi: 10.1016/j.bios.2013.09.051.

[15] P. Béland, O. Krupin, et P. Berini, « Selective detection of bacteria in urine with a long-range surface plasmon waveguide biosensor », *Biomed. Opt. Express*, vol. 6, nº 8, p. 2908, août 2015, doi: 10.1364/BOE.6.002908.

[16] M. Khodami et P. Berini, « Biomolecular kinetics analysis using long-range surface plasmon waveguides », *Sensors and Actuators B: Chemical*, vol. 243, p. 114-120, mai 2017, doi: 10.1016/j.snb.2016.11.120.

[17] A. E. Cetin *et al.*, « Handheld high-throughput plasmonic biosensor using computational on-chip imaging », *Light Sci Appl*, vol. 3, nº 1, p. e122-e122, janv. 2014, doi: 10.1038/lsa.2014.3.

[18] J. Dostálek, J. Homola, et M. Miler, « Rich information format surface plasmon resonance biosensor based on

array of diffraction gratings », *Sensors and Actuators B: Chemical*, vol. 107, nº 1, p. 154-161, mai 2005, doi: 10.1016/j.snb.2004.08.033.

[19] J. Homola, I. Koudela, et S. S. Yee, « Surface plasmon resonance sensors based on diffraction gratings and prism couplers: sensitivity comparison », *Sensors and Actuators B: Chemical*, vol. 54, nº 1-2, p. 16-24, janv. 1999, doi: 10.1016/S0925-4005(98)00322-0.

[20] P. Berini, « Bulk and surface sensitivities of surface plasmon waveguides », *New J. Phys.*, vol. 10, nº 10, p. 105010, oct. 2008, doi: 10.1088/1367-2630/10/10/105010.

[21] H. Cai, M. Wang, J. Liu, et X. Wang, « Theoretical and experimental study of a highly sensitive SPR biosensor based on Au grating and Au film coupling structure », *Opt. Express*, vol. 30, nº 15, p. 26136, juill. 2022, doi: 10.1364/OE.461768.

[22] S. Nazem, M. Malekmohammad, et M. Soltanolkotabi, « Theoretical and experimental study of a surface plasmon sensor based on Ag-MgF2 grating coupler », *Appl. Phys. B*, vol. 126, nº 5, p. 96, mai 2020, doi: 10.1007/s00340-020-07449-w.

[23] J. Cao, Y. Sun, Y. Kong, et W. Qian, « The Sensitivity of Grating-Based SPR Sensors with Wavelength Interrogation », *Sensors*, vol. 19, nº 2, p. 405, janv. 2019, doi: 10.3390/s19020405.

[24] J. González-Colsa, G. Serrera, J. M. Saiz, F. González, F. Moreno, et P. Albella, « On the performance of a tunable grating-based high sensitivity unidirectional plasmonic sensor », *Opt. Express*, vol. 29, nº 9, p. 13733, avr. 2021, doi: 10.1364/OE.422026.

[25] A. Shalabney et I. Abdulhalim, « Sensitivity-enhancement methods for surface plasmon sensors: SPR sensors sensitivity enhancement », *Laser & Photon. Rev.*, vol. 5, nº 4, p. 571-606, juill. 2011, doi: 10.1002/lpor.201000009.

[26] M. Piliarik et J. Homola, « Surface plasmon resonance (SPR) sensors: approaching their limits? », *Opt. Express*, vol. 17, nº 19, p. 16505, sept. 2009, doi: 10.1364/OE.17.016505.

[27] D. Cai, Y. Lu, K. Lin, P. Wang, et H. Ming, « Improving the sensitivity of SPR sensors based on gratings by double-dips method (DDM) », *Opt. Express*, vol. 16, nº 19, p. 14597, sept. 2008, doi: 10.1364/OE.16.014597.

[28] A. V. Kabashin, S. Patskovsky, et A. N. Grigorenko, « Phase and amplitude sensitivities in surface plasmon resonance bio and chemical sensing », *Opt. Express*, vol. 17, nº 23, p. 21191, nov. 2009, doi: 10.1364/OE.17.021191.

[29] R. Slavík et J. Homola, « Ultrahigh resolution long range surface plasmon-based sensor », *Sensors and Actuators B: Chemical*, vol. 123, nº 1, p. 10-12, avr. 2007, doi: 10.1016/j.snb.2006.08.020.

[30] J. Sauvage-Vincent, Y. Jourlin, V. Petiton, A. V. Tishchenko, I. Verrier, et O. Parriaux, « Low-loss plasmon-triggered switching between reflected free-space diffraction orders », *Opt. Express*, vol. 22, nº 11, p. 13314, juin 2014, doi: 10.1364/OE.22.013314.

[31] A. V. Tishchenko et O. Parriaux, « Coupled-Mode Analysis of the Low-Loss Plasmon-Triggered Switching Between the 0 th and -1 st Orders of a Metal Grating », *IEEE Photonics J.*, vol. 7, nº 4, p. 1-9, août 2015, doi: 10.1109/JPHOT.2015.2445766.

[32] H. Bruhier *et al.*, « Effect of roughness on surface plasmons propagation along deep and shallow metallic diffraction gratings », *Opt. Lett.*, vol. 47, nº 2, p. 349, janv. 2022, doi: 10.1364/OL.443659.

[33] E. Laffont, N. Crespo-Monteiro, A. Valour, P. Berini, et Y. Jourlin, « Differential Sensing with Replicated Plasmonic Gratings Interrogated in the Optical Switch Configuration », *Sensors*, vol. 23, nº 3, p. 1188, janv. 2023, doi: 10.3390/s23031188.

[34] E. Laffont, A. Valour, N. Crespo-Monteiro, P. Berini, et Y. Jourlin, « Biosensing in the optical switch configuration on strong plasmonic gratings enabling differential referenced detection », *Sensing and Bio-Sensing Research*, vol. 45, p. 100681, août 2024, doi: 10.1016/j.sbsr.2024.100681.

[35] H. Bruhier *et al.*, « Quasi-lossless common-mode plasmon sensing scheme as a high sensitivity compact SPR sensor », *Opt. Lett.*, juin 2023, doi: 10.1364/OL.483692.

[36] L. Bsawmaii *et al.*, « Magneto-plasmonic “switch” device for magnetic field detection », *Nanophotonics*, vol. 13, nº 19, p. 3689-3698, août 2024, doi: 10.1515/nanoph-2024-0136.

[37] U. Fano, « The Theory of Anomalous Diffraction Gratings and of Quasi-Stationary Waves on Metallic Surfaces (Sommerfeld’s Waves) », *J. Opt. Soc. Am.*, vol. 31, nº 3, p. 213, mars 1941, doi: 10.1364/JOSA.31.000213.

[38] V. G. Achanta, « Surface waves at metal-dielectric interfaces: Material science perspective », *Reviews in Physics*, vol. 5, p. 100041, nov. 2020, doi: 10.1016/j.revip.2020.100041.

[39] S. A. Maier, *Plasmonics: fundamentals and applications*. New York, NY: Springer, 2010.

[40] J. M. Pitarke, V. M. Silkin, E. V. Chulkov, et P. M. Echenique, « Theory of surface plasmons and surface-plasmon polaritons », *Rep. Prog. Phys.*, vol. 70, nº 1, p. 1-87, janv. 2007, doi: 10.1088/0034-4885/70/1/R01.

[41] R. W. Wood, « On a Remarkable Case of Uneven Distribution of Light in a Diffraction Grating Spectrum », *Proc. Phys. Soc. London*, vol. 18, nº 1, p. 269-275, juin 1902, doi: 10.1088/1478-7814/18/1/325.

[42] J. Chandezon, G. Raoult, et D. Maystre, « A new theoretical method for diffraction gratings and its numerical application », *J. Opt.*, vol. 11, nº 4, p. 235-241, juill. 1980, doi: 10.1088/0150-536X/11/4/005.

[43] L. Li, J. Chandezon, G. Granet, et J.-P. Plumey, « Rigorous and efficient grating-analysis method made easy for optical engineers », *Appl. Opt.*, vol. 38, nº 2, p. 304, janv. 1999, doi: 10.1364/AO.38.000304.

[44] N. Lyndin et B. Usievich, *MC Grating*. (2013). [Windows 10]. Disponible sur: https://mcgrating.com/

[45] S. Rossi, E. Gazzola, P. Capaldo, G. Borile, et F. Romanato, « Grating-Coupled Surface Plasmon Resonance (GC-SPR) Optimization for Phase-

Interrogation Biosensing in a Microfluidic Chamber », *Sensors*, vol. 18, nº 5, p. 1621, mai 2018, doi: 10.3390/s18051621.

[46] J. Homola, « Surface Plasmon Resonance Sensors for Detection of Chemical and Biological Species », *Chem. Rev.*, vol. 108, nº 2, p. 462-493, févr. 2008, doi: 10.1021/cr068107d.

[47] K. Ichihashi, Y. Mizutani, et T. Iwata, « Enhancement of the sensitivity of a diffraction-grating-based surface plasmon resonance sensor utilizing the first-and negative-second-order diffracted lights », *OPT REV*, vol. 21, nº 5, p. 728-731, sept. 2014, doi: 10.1007/s10043-014-0119-5.

[48] S. Afsheen *et al.*, « Modeling of 1D Au plasmonic grating as efficient gas sensor », *Mater. Res. Express*, vol. 6, nº 12, p. 126203, nov. 2019, doi: 10.1088/2053-1591/ab553b.

[49] D. Jang, G. Chae, et S. Shin, « Analysis of Surface Plasmon Resonance Curves with a Novel Sigmoid-Asymmetric Fitting Algorithm », *Sensors*, vol. 15, nº 10, p. 25385-25398, sept. 2015, doi: 10.3390/s151025385.

[50] K. Kurihara, K. Nakamura, et K. Suzuki, « Asymmetric SPR sensor response curve-fitting equation for the accurate determination of SPR resonance angle », *Sensors and Actuators B: Chemical*, vol. 86, nº 1, p. 49-57, août 2002, doi: 10.1016/S0925-4005(02)00146-6.

[51] S. Bellucci, O. Vernyhor, A. Bendziak, I. Yaremchuk, V. M. Fitio, et Y. Bobitski, « Characteristics of the Surface Plasmon–Polariton Resonance in a Metal Grating, as a Sensitive Element of Refractive Index Change », *Materials*, vol. 13, nº 8, p. 1882, avr. 2020, doi: 10.3390/ma13081882.

[52] E. Popov, L. Tsonev, et D. Maystre, « Losses of Plasmon Surface Waves on Metallic Grating », *Journal of Modern Optics*, vol. 37, nº 3, p. 379-387, mars 1990, doi: 10.1080/09500349014550431.

[53] E. I. Jury, *Theory and application of the z-transform method*. Huntington, N.Y: R. E. Krieger Pub. Co, 1973.

[54] P. Virtanen *et al.*, « SciPy 1.0: fundamental algorithms for scientific computing in Python », *Nat Methods*, vol. 17, nº 3, p. 261-272, mars 2020, doi: 10.1038/s41592-019-0686-2.

[55] S. W. Smith, *The scientist and engineer's guide to digital signal processing*, 1st ed. San Diego, Calif: California Technical Pub, 1997.

[56] K. M. McPeak *et al.*, « Plasmonic Films Can Easily Be Better: Rules and Recipes », *ACS Photonics*, vol. 2, nº 3, p. 326-333, mars 2015, doi: 10.1021/ph5004237.

[57] M. Daimon et A. Masumura, « Measurement of the refractive index of distilled water from the near-infrared region to the ultraviolet region », *Appl. Opt.*, vol. 46, nº 18, p. 3811, juin 2007, doi: 10.1364/AO.46.003811.

[58] S. Long *et al.*, « Grating coupled SPR sensors using off the shelf compact discs and sensitivity dependence on grating period », *Sensors and Actuators Reports*, vol. 2, nº 1, p. 100016, nov. 2020, doi: 10.1016/j.snr.2020.100016.

[59] Y. Dai, H. Xu, H. Wang, Y. Lu, et P. Wang, « Experimental demonstration of high sensitivity for silver rectangular grating-coupled surface plasmon resonance (SPR) sensing », *Optics Communications*, vol. 416, p. 66-70, juin 2018, doi: 10.1016/j.optcom.2018.02.010.